Check for updates

N,N-Dimethylpyridin-4-amine (DMAP) based ionic liquids: evaluation of physical properties *via* molecular dynamics simulations and application as a catalyst for Fisher indole and 1H-tetrazole synthesis†

Sarfaraz Ali Ghumro,‡[a] Sana Saleem,‡[a] Mariya al-Rashida, [b] Nafees Iqbal,[a] Rima D. Alharthy,[c] Shakil Ahmed,[a] Syed Tarique Moin*[a] and Abdul Hameed*[a]

The last few decades have seen a rapid increase in the use of ionic liquids (ILs) as a green alternative to traditional solvents in organic synthesis. The use of ILs as catalysts has also increased in recent years. Herein we the report synthesis of new N,N-dimethylpyridin-4-amine (DMAP) based ionic liquids (ILs) as new and efficient catalysts for the facile synthesis of indoles (*via* Fischer indole synthesis), and 1H-tetrazoles (*via* click chemistry). The method is environmentally friendly, requiring only minimum catalyst loading (0.2 equiv. for Fischer indole synthesis). In the case of 1H-tetrazole formation (*via* click chemistry), the reaction was carried out under a solvent free environment. Moreover, thermal studies (TGA, DTG and DSC) of DMAP-ILs (2, 3) have also been carried out to elicit their stability for temperature dependent reactions. Application of molecular dynamics simulations provided valuable insights into the structural and transport properties of these ionic liquids. An MP2 method was applied to evaluate the stability of the compound *via* binding energy calculations.

1. Introduction

Although the concept of ionic liquids (ILs) has been around for more than a hundred years, a sudden surge in the interest of applications of ILs in both academia and industry has only been witnessed in the last three decades or so.[1–5] Traditionally, ILs were defined as salts being made up of positively and negatively charged ions that are liquid at temperatures typically below 100 °C.[2] However strict adherence to this criteria of an IL being liquid at temperature below 100 °C is no longer valid, and many high temperature ILs are also known.[6] ILs are widely regarded as "designer liquids", where, according to the particular application, individual cationic or anionic moieties can be independently selected allowing us to tailor the physiochemical properties of ILs as desired, thereby introducing flexibility in

the design and applications of ILs.[7] The use of ILs as catalyst for organic syntheses has increased in the recent past. The ideal properties of ILs, such as low volatility, high thermal stability, and ease of re-cyclization further adds to their appeal.[2,8] Nitrogen containing cationic scaffolds, typically pyridine or imidazole, with various counter ions have been widely employed for catalyzing different organic reactions.[9] However, imidazole's inert nature[10] and extreme toxicity, and volatility of pyridine impedes their utilization in organic syntheses and urges the discovery and development of new ionic liquids with less toxic cations. N,N-Dimethylpyridin-4-amine (DMAP), is a pyridine based non-volatile, crystalline reagent. It has been extensively used as a catalyst in organic syntheses, especially in coupling reactions, such as esterification, amide formation and for protecting functional groups (*i.e.* TBS, Boc) (Fig. 1).[11,12]

In the present study, we have synthesized new DMAP-based ionic liquids *via* N-alkylation, and successfully employed them as catalyst for Fisher indole/indolenine and 1H-tetrazole formation. To the best of our knowledge, DMAP-based ionic liquids have neither been synthesized nor employed as catalyst to mediate organic reactions. The commercially available DMAP was treated with alkyl bromide to get the corresponding N-alkylated cations with bromide anions. Owing to the documented nature of fluoride ions as catalyst and as a mild base in various organic reactions,[13] the afore mentioned N-alkylated cations with bromide ions were subjected to anion exchange

[a]H. E. J. Research Institute of Chemistry, International Center for Chemical and Biological Sciences, University of Karachi, Karachi-75270, Pakistan. E-mail: tarique. syed@iccs.edu; abdul.hameed@iccs.edu; Fax: +92-21-3481901; Tel: +92-21-99261774; +92-21-99261701-2

[b]Department of Chemistry, Forman Christian College, A Chartered University, Ferozepur Road-54600, Lahore, Pakistan

[c]Department of Chemistry, Science and Arts College, Rabigh Campus, King Abdulaziz University, Jeddah, Saudi Arabia

† Electronic supplementary information (ESI) available: NMR spectra of the synthesized compounds. See DOI: 10.1039/c7ra06824g
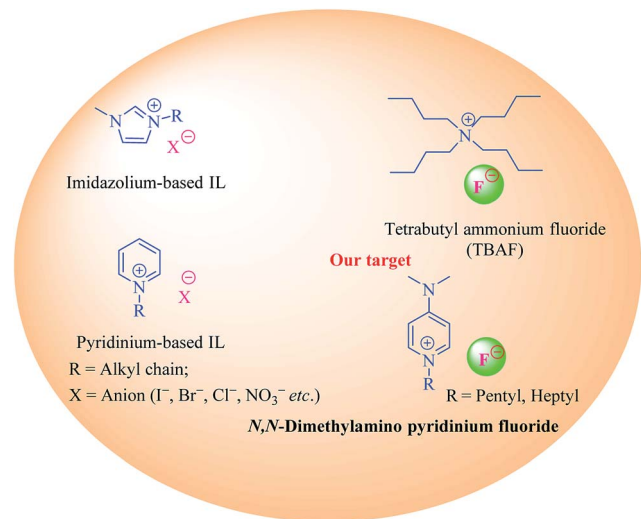
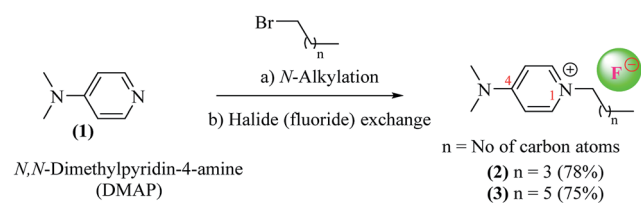‡ Shared first author (contributed equally).

(a)

89% **(6a)**

78% **(6b)**

74% **(6c)**

56% **(6d)**

76% **(6e)**

45% **(6f)**

55% **(6g)**

17% **(6h)**

Fig. 1 Structures of imidazolium, pyridinium, TBAF and *N,N*-dimethylamino pyridinium fluoride.

Scheme 1 Synthesis of DMAP-based ionic fluoride salts. Reaction conditions: (a) pentyl or heptyl bromides, toluene, heated at reflux (118–120 °C); (b) treatment with silver fluoride aqueous solution.

(b)

48% **(8a)**

78% **(8b)**

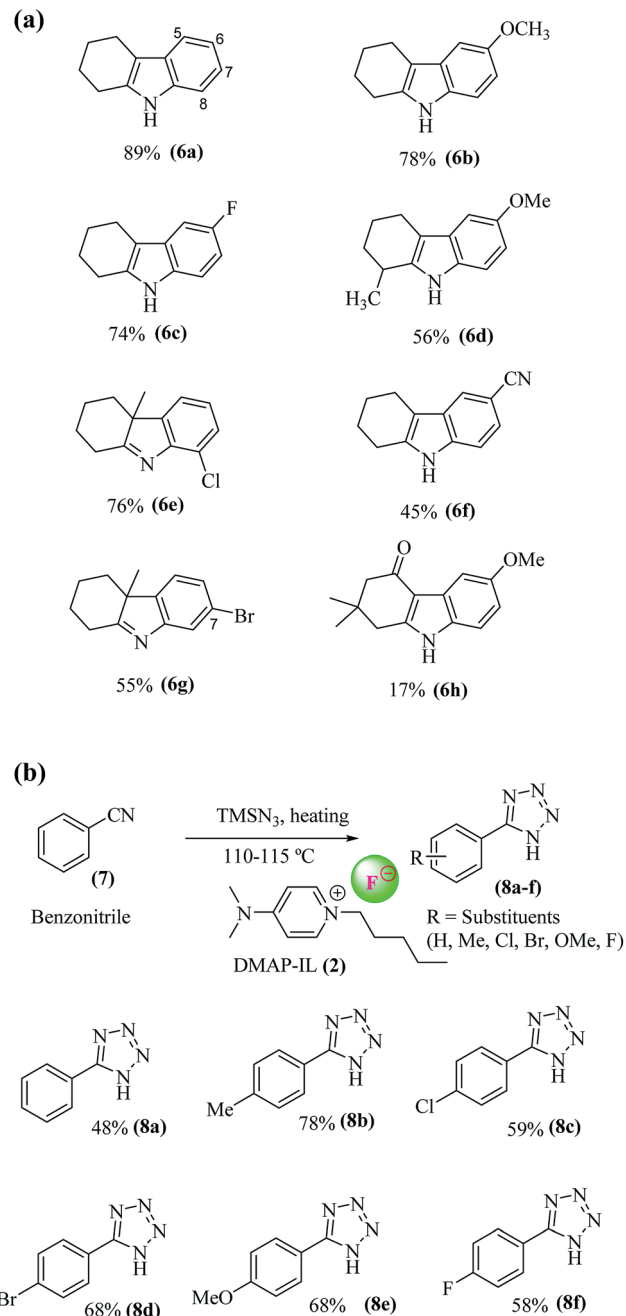59% **(8c)**

68% **(8d)**

68% **(8e)**

58% **(8f)**

Fig. 2 (a) Structures of different substituted tetrahydro-1*H*-carbazole (indoles)/methyl tetrahydro-1*H*-carbazole (indolenines). Note: all the reactions have been carried out by using DMAP-IL (**2**) catalyst (0.2 equiv.) in ethanol. (b) DMAP-IL catalyzed synthesis of substituted 1*H*-tetrazoles (**8a–f**).

with fluoride ions. The resulting DMAP-IL (dimethylamino pyridinium with fluoride counter anion) could effectively serve as a substitute for tetra butyl ammonium fluoride (TBAF), a well-known catalyst and IL that has been used to promote different chemical reactions (Scheme 1).[13–15] The DMAP-based ionic liquids (**2**, **3**) with fluoride counter anions were then investigated for their efficiency as catalysts for synthesis of tetrahydro-1*H*-carbazole (indoles)/methyl tetrahydro-1*H*-carbazole (indolenines) (Fig. 2a) and 1*H*-tetrazole (Fig. 2b) compounds.

Indole is a bicyclic hetero-aromatic scaffold which serves as an important structural component in many medicinally important compounds such as serotonin, melatonin, alosetron *etc.*[16] For the synthesis of this important scaffold, a number of synthetic protocols have been reported, however, Fisher indole synthesis remains one of the most popular and significant methods. A typical method involves coupling of a ketone with arylhydrazine to from an arylhydrazone, with subsequent release of ammonia *via* [3,3]-sigmatropic arrangement under acidic conditions to furnish the indole ring. Since the development of indol formation by Fisher, a range of different catalysts such as protic acids (H₂SO₄, polyphosphoric acid, HCl, AcOH), Lewis acids (TiCl₄, ZnCl₂, PCl₃), and imidazole[17] or pyridine[18] based ionic liquids, have been used to catalyze indole synthesis. Recently low melting mixtures, also called deep

eutectic solvents (DES), have also been used to carry out indole formation.[19] In these reactions, the low melting mixture (DES) was used in large quantity, *i.e.* up to a gram in one mmol scale reaction, adding dreariness to its removal from the reaction mixture. In the present study, we prepared new DMAP-based ionic liquids (Scheme 1) and successfully employed them as catalysts with minimum loading in indole formation (Table 1, Fig. 2a). In addition, DMAP-ILs has also be used to perform click

Table 1 Optimization of Fisher indole synthesis using DMAP-ILs

Entry	DMAP-ILs	Equivalent[a]	% yield (6a)
1	2	0.05	68
2	2	0.2	89
3	2	0.3	91
4	3	0.05	48
5	3	0.2	64

[a] Catalytic amount of DMAP-ILs in ethanol.

reaction for 1*H*-tetrazole synthesis under solvent-free conditions.

Tetrazole is a nitrogen containing, five membered ring which serves as an isosteric substituent of carboxylic acid. It serves as important structural component in several molecules of pharmaceutical interest.[20] The presence of 1*H*-tetrazole species in drug molecules has been known to favorably enhance their metabolic resistance and pharmacokinetic properties.[21] Tetrazoles have been found significant importance in coordination chemistry, as well as they have also shown great importance in a large number of synthetic transformations as intermediates.[22–24] Being an analog and metabolically stable substitute of a carboxyl group, the tetrazole ring is extensively used in molecular design and in the synthesis of modified amino acids and peptidomimetics.[22,25] This area of chemistry has strong impact since the last two decades emphasizing on the popular synthesis and applications of tetrazoles.[26,27]

The term click chemistry was introduced by Sharpless *et al.* by preforming [2 + 3] cycloaddition between nitrile and azide moieties to form the tetrazole.[28] The tetrazole formation reaction was usually catalyzed by using zinc metal,[29–31] however, Amantini *et al.* developed metal free conditions for click reaction. They used tetrabutyl ammonium fluoride (TABF) as catalyst for tetrazole formation by reacting nitrile species with trimethylsilyl azide.[15] In the context of developing metal free click reaction of tetrazole formation, we synthesized new *N,N*-dimethylamino pyridinium cation with fluoride anion as alternate of TBAF in 1*H*-tetrazole synthesis due to their easy handling and rapid preparation from commercially available solid 4-dimethylaminopyridine. The new DMAP-based ionic liquids were successfully employed them as catalysts with minimum loading (0.2 equivalent) tetrazole formation. Moreover, the removal of DMAP-based ionic liquids from the reaction mixture was also found easy. The catalytic efficiency of DMAP-IL (2) in click chemistry of 1*H*-tetrazole formation was explored by reacting different benzonitriles with azide source, *i.e.* trimethylsilyl azide, under solvent-free conditions (Fig. 2b).

Ionic liquids have a wide range of applications in different disciplines including energy and biological sciences and the evaluation of physical properties of ionic liquids such as viscosity, melting point, boiling point *etc.* must be known prior to their applications. To evaluate these properties for the related applications a rational approach based on systematic methods is needed to design efficient ionic liquids consisting of appropriate ionic pairs. Among such properties, the transport

properties vary significantly when subtle changes are made in the structure of cation and anion pairs.[32] Other properties such as viscosity and conductance depends on the diffusivity of ions *i.e.* viscosity becomes low and conductance gets higher, as the diffusion of ions is fast, therefore, the estimation of diffusion of ions would be helpful for the designing of new ionic liquids.[33] Both structural and transport properties were extensively studied *via* molecular dynamics (MD) simulations.[34,35] The simulation methods were successfully applied to obtain reliable information related to both structure and transport properties of ionic liquids. Self-diffusion properties were recently reported for newly synthesized quinolone based ionic fluoride salts (QuFs) using molecular dynamics simulations.[36] A similar procedure was adopted to evaluate structure and transport properties of DMAP based ionic liquids in bulk. Self-diffusion coefficients and viscosities of these ionic liquids were also computed. The stability of ionic liquids is of prime importance, therefore, binding energies were computed for the DMAP ionic liquids using the second order Møller–Plesset (MP2) perturbation theory method.

2. Results and discussion

2.1. Chemistry

A general scheme for the preparation of DMAP-based ionic liquids (DMAP-ILs) comprises of two steps *i.e.* (a) *N*-Alkylation of dimethylamino pyridine (DMAP), and (b) exchange of bromide counter anion with fluoride anion. The yields of final DMAP-ILs (2, 3) with fluoride counter anion were found to be 78% and 75%, respectively (Scheme 1). The newly synthesized DMAP-ILs were then employed as catalyst in organic synthesis; (1) Fisher indole synthesis and (2) 1*H*-tetrazole formation. The catalyst (2, 3) can be easily removed *via* simple aqueous work-up from the reaction mixture.

A typical reaction of Fisher indole synthesis, between phenyl hydrazine and cyclohexanone, was carried out by using DMAP-based ionic liquids as catalyst, in ethanol as a solvent, affording the desired product 7 in excellent yield. The reaction conditions were optimized by varying the amount of DMAP-IL catalysts (2, 3) as shown in Table 1. The percentage yield (89%) of corresponding indole (2,3,4,9-tetrahydro-1*H*-carbazole) up on addition of 0.2 equiv. of DMAP based IL (2), was found to be comparable to the yield (91%) obtained while using 0.3 equiv. of DMAP-IL. Accordingly, DMAP-based ionic liquid (2) as catalyst
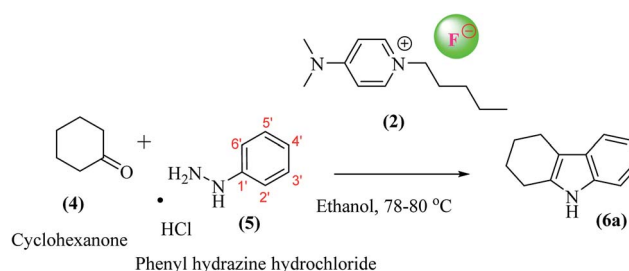
Scheme 2 Fisher indole synthesis using DMAP-IL as catalyst (2).

with 0.2 equiv. was opted for further investigating the scope of DMAP-based catalyst (Scheme 2).

By utilizing the optimized conditions, a range of different substituted phenyl hydrazine hydrochlorides were treated with cyclohexanone or 2-methyl cyclohexanone to furnish the corresponding tetrahydro-1*H*-carbazole (indoles)/methyl tetrahydro-1*H*-carbazole (indolenines) derivatives (**6a–h**) in variable yields (Fig. 2a). No indole formation was observed in case of 2,4-dinitrophenyl hydrazine even on increasing the temperature (up to 100 °C) and reaction time to 14 h. It may be due to the electron withdrawing effects of nitro groups which hampered the requisite cyclization of phenyl ring with cyclohexane to complete the corresponding indole scaffold. However, the reaction occurred smoothly with phenyl hydrazine, 4′-methoxy and 4′-fluorophenyl hydrazine to afford indoles **6a** (89%), **6b** (78%) and **6c** (75%) in good yields. The slight low yield (75%) of 6′-fluoro substituted indole **6c** may be due to electron withdrawing effect of fluoro substituent. The reaction of 2-methyl cyclohexanone with methoxyphenyl hydrazine in the presence of catalyst (**2**) yielded corresponding indole (**6d**) in modest yields (56%). While the reaction of 2-methyl cyclohexanone with 2′-chloro substituted phenyl hydrazine gave corresponding 8′-chloro indolenine (**6e**) in 76% and with 3′-bromo substituted phenyl hydrazine afforded 7′-bromo indolenine (**6g**) as a major regioisomeric product in 55% yield. The reaction of 4′-cyano substituted phenyl hydrazine with cyclohexanone produce corresponding indole (**6f**) in moderate yield (60%) due to strong electron withdrawing effect of cyano group yield. The reaction of 1,3-cyclohexanediones (dimedone) with phenylhydrazine, gave low yield (17%) of corresponding indole (**6h**) due to the formation of stable *N*-phenylhydrazone intermediate which is difficult to activate for the next [3,3] sigmatropic rearrangement to furnish the corresponding indole (**6h**) (Fig. 2a).

Further, the click reaction of 1*H*-tetrazole formation between benzonitrile and trimethylsilyl azide (TMSN$_3$) was carried out in the presence of DMAP-IL (0.3 equiv.) as a catalyst. The reaction occurred smoothly and gave the desired 1*H*-tetrazole in good to moderate yield (78–48%). TMSN$_3$ was used as an azide source. Because of fluoride anion's greater affinity for silyl group, there is a much more efficient release of active azide for click reaction of tetrazole formation.[15,37] To further broaden the scope of DMAP-based ionic fluoride liquid (**2**) as a catalyst, click reactions with different substituted benzonitriles and TMSN$_3$ were carried out. In all cases, the 1*H*-phenyl tetrazoles (**8a–f**) were obtained in good yields. The yield of unsubstituted phenyl tetrazole (**8a**, 48%) was found low in comparison to methyl substituted phenyl tetrazole (**8b**, 78%). This could be due to electron donating effect of methyl group which enhanced the reactivity of cyano group. The yields of halogen substituted (Cl, Br, F) phenyl tetrazoles (**8c**, 59%), (**8d**, 68%), and (**8f**, 58%) were found less compared to (**8b**). This is due to electron withdrawing effect of halogen substituents. Further among halogen substituted phenyl tetrazoles, the percentage yield with more electronegative substituents F and Cl was found to be less as compared to least electronegative substituents Br. The yield of methoxy substituent bearing phenyl tetrazole (**8e**) was also found to be good (70%). The structures of synthesized
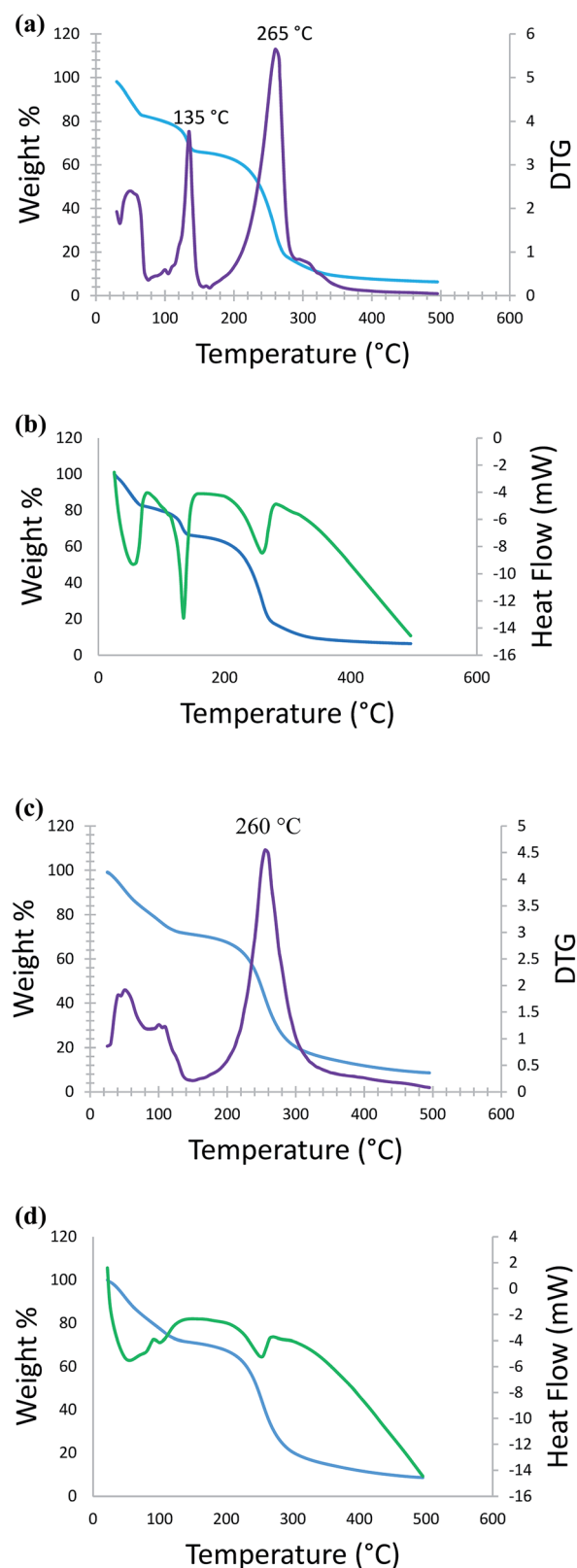

Fig. 3 DMAP-IL **2**, (a) overlap of TGA (blue) and DTG (purple) graphs; (b) overlap of TGA (blue) and DSC (green) graphs: DMAP-IL **3**, (c) overlap of TGA (blue) and DTG (purple) graphs; (d) overlap of TGA (blue) and DSC (green) graphs.

compounds **8a–f** were confirmed with NMR spectroscopy and mass spectrometry (Fig. 2b).

2.2. Thermal studies

Thermal studies of DMAP-ILs (**2**, **3**) were also conducted to signify the efficiency of catalyst in temperature dependent reactions. Thermal stability and decomposition pattern was evaluated by carrying out thermogravimetric analysis (TGA), derivative thermogravimetry (DTG), and differential scanning calorimetry (DSC) (Fig. 3). Fig. 3a shows overlap of thermogravimetric (TGA) graph and its first derivative (DTG) for compound (**2**), and Fig. 3b shows overlap of TGA and DSC graphs. In the first step, there is a gradual loss of weight (16%), in the temperature range from ambient to 70 °C, this is probably due to the loss of water molecules. Immediately after this step, the onset of degradation is observed in the temperature range 70 °C to 140 °C where weight loss of 16% is observed, from DTG the first decomposition temperature appears at 135 °C. In the third and final step remaining weight loss (60%) is observed in the range 140 °C to 310 °C, the decomposition temperature for this step is observed at 265 °C. All three weight loss steps are accompanied by an endothermic change as can be seen from the DSC data (Fig. 3). Similarly, the thermal analysis (TGA, DTG and DSC) of compound **3** data has been obtained. Consequently, Fig. 3c shows overlap of thermogravimetric (TGA) graph and its first derivative (DTG) and Fig. 3d shows overlap of TGA and DSC graphs. As the compound is heated from ambient temperature to 140 °C a weight loss of 32% is observed, this is most likely due to the loss of water. After this step, the decomposition is observed in the temperature range from 200 °C to 340 °C, during which the remaining weight loss (52%) is observed. The decomposition temperature calculated from DTG is 260 °C. This step is accompanied by an endothermic change as can be seen from the DSC data (Fig. 3d).

2.3. Theoretical studies of DMAP-IL (2, 3)

2.3.1. Bulk properties. Molecular dynamics simulations were carried out to investigate the bulk properties of DMAP
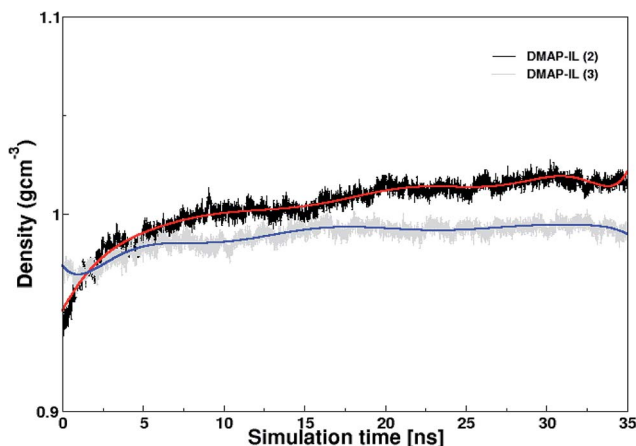

Fig. 4 Densities of DMAP (**2**) and (**3**) ionic liquids as a function of simulation time.
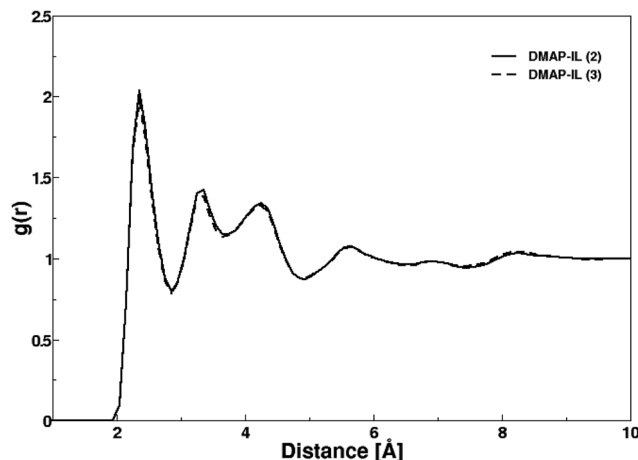

Fig. 5 Radial distribution functions between center of masses of cation and anion in both DMAP ionic liquids.

based ionic liquids, such as density, structural and transport properties which could further help in expanding the application of DMAP-based ionic liquids. Similarly, the newly synthesized DMAP based ionic liquids demonstrated their significances as catalysts, yet further applications of these ionic liquids would depend on the bulk properties which were evaluated *via* molecular dynamics simulations. Fig. 4 illustrates variation of densities of DMAP-ILs (**2**) and (**3**) at room temperature as a function of time. Average densities of 1.00 ± 0.02 and 0.99 ± 0.02 g cm^{-3} were obtained for DMAP-ILs (**2**) and (**3**) at room temperature, thus showing no effect of the alkyl chain lengthening in the two ionic liquids.

The structural attributes of DMAP ILs (**2**) and (**3**) were primarily analyzed *via* radial distribution functions (RDFs) plotted between center of mass of cations and anions *i.e.* pyridinium and fluoride ions. Fig. 5 depicts the RDF profiles of cation–anion interaction in both cases, minimal distances of 2.35 Å were deduced from the first peak of both RDFs. The RDF patterns were very much similar to that of quinoline based ionic liquids previously investigated by us,[36] thus demonstrating that the size and structural features of the cation had no significant influence on the cation–anion interaction. The first peaks were continued to well-structured second and third shell peaks at 3.32 and 4.26 Å along with few more peaks showing a long range influence of cations on anion or *vice versa*. A very sharp first peak was attributed to the strong electrostatic attraction between cations and their respective anions whereas second and third peak with low density corresponded to electrostatic interaction between cations and anions of opposite ion pairs.

To further resolve the characteristic differences between the two DMAP ionic liquids *i.e.* compounds **2** and **3**, RDFs were plotted between atomic pairs of cations and anions as shown in Fig. 6. The distribution function between nitrogen atoms of pyridinium ion and fluoride ions (g_{C-A}) in DMAP ILs (**2**) and (**3**) exhibited identical well-defined first peaks with maxima at 3.75 Å, which demonstrates the strong attraction between cations and anions based on electrostatics forces. A difference in the g_{C-A} profile of the two ionic liquids was observed, and that
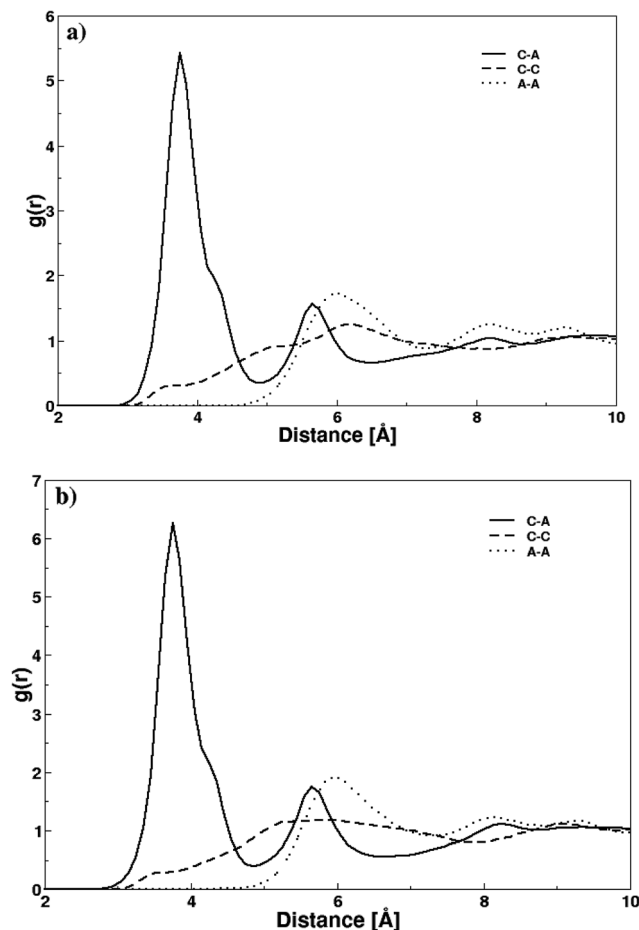
Fig. 6 (a) Radial distribution functions between N atoms of pyridinium ions (C−C), between fluoride ions (A−A) and between the N atoms of pyridinium ions and fluoride ion (C−A) of the DMAP (2) ionic liquids; (b) radial distribution functions between N atoms of pyridinium ions (C−C), between fluoride ions (A−A) and between the N atoms of pyridinium ions and fluoride ion (C−A) of the DMAP (3) ionic liquids.

difference was a bit higher intensity of the first peak in case of DMAP (3), as compared to its corresponding DMAP derivative. The $g_{C–A}$ profile yielded a tiny shoulder peak at ~4.35 Å along with the first peak which was attributed to the electron delocalization of the dimethyl amine attached to pyridinium ring that undergoes isomerization to produce dimethyl ammonium ion – a typical isomer of DMAP which may interact with fluoride ions and is involved in a number of catalytic reactions. Moreover, a similar trend was observed in the distribution functions of both ionic liquids between nitrogen atoms of pyridinium ions ($g_{C–C}$) and fluoride ($g_{A–A}$) ions – no peak was observed in the $g_{C–C}$ profile indicating no structure ordering of the pyridinium ions which may be due to strong repulsion between cations whereas first peak appeared at 5.96 Å in case of $g_{A–A}$ profile of fluoride ions.

Both ionic liquids presented identical structural properties evaluated *via* radial distribution functions, nevertheless it was significant to assess the effect of alkyl chain length that was made possible by the evaluation of radius of gyration (R_g) of the two ionic liquids. Fig. 7 depicts the distribution of the radius of
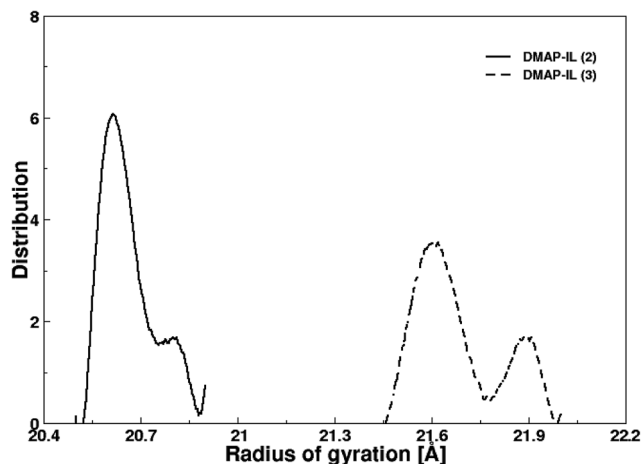

Fig. 7 Radius of gyration in DMAP based ionic liquids.

gyration obtained from MD simulation of DMAP ILs (2) and (3). The R_g distribution plot yielded the most probable values of 20.6 and 21.6 Å for DMAP (2) and (3), respectively. In both plots, shoulder peaks were visible at 20.8 and 21.9 Å showing the flexibility of alkyl side chain of different length. This further encouraged us to evaluate the transport properties of both ionic
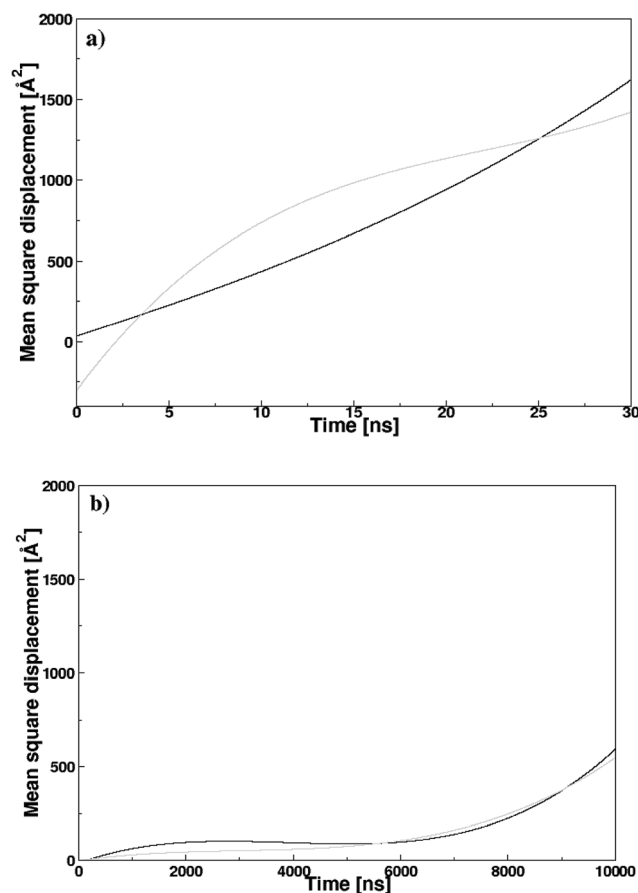

Fig. 8 Mean-square displacement (MSDs) of the pyridinium and fluoride ions in the (a) DMAP (2) and (b) DMAP (3) ionic liquids; black and gray lines are for the cation and anion, respectively.

liquids, since transport properties were reported to be dependent on the alkyl side chain attached to core structure of different scaffolds.

Fig. 8 illustrates the mean square displacement (MSD) of the pyridinium and fluoride ions in the DMAP ILs (2) and (3), as obtained from MD simulations. The influence of alkyl chains of different length on the transport properties of DMAP based ionic liquids were demonstrated *via* MSD analysis that produced asymptotic plots similar to those observed in case of quinolinium based ionic liquids. The transport properties of cations with two different alkyl chains were reported to affect the properties of anions, therefore, a somewhat similar behavior was presumed for DMAP based ionic liquids. The MSD plots for the two ionic liquids presented a contrasting behavior, since the mean square displacement of both ions in the DMAP (2) was higher, indicating the fast motion of the alkyl side chain (*cf.* Fig. 8a). For the DMAP (3), the alkyl side chain did not follow the same trend, since low chain motion was deduced from the MSD plot shown in Fig. 8b. This could be due to strong electrostatic interactions between cations and anions thus resulting in ionic packing and restricting the fast motion of the alkyl chain. From the MSD plot, self-diffusion coefficients (*D*) were computed using the Einstein relation.

$$2nD = \lim_{t \to \infty} \left(\frac{\text{MSD}}{t} \right)$$

where *n* denotes the number of dimensions and it is equal to 3 in these cases whereas *D* represents diffusion coefficient.

Applying fitting procedure to the MSD plots with asymptotic linear region up to 2 ns corresponding to diffusion properties for pyridinium and fluoride ions, self-diffusion coefficients (*D*) were computed from the MSD slopes overs 0–2 ns. The coefficient values for pyridinium and fluoride ions in DMAP (2) were computed as $1.92 \pm 0.01 \times 10^{-6}$ and $6.09 \pm 0.14 \times 10^{-6}$ cm^2 s^{-1}, respectively. In case of DMAP IL (3), comparatively low values of self-diffusion coefficients were obtained ($0.92 \pm 0.06 \times 10^{-6}$ and $0.38 \pm 0.03 \times 10^{-6}$ cm^2 s^{-1} for pyridinium and fluoride ions, respectively). The coefficient value of the fluoride ion in DMAP IL (3) was lower in comparison to that of DMAP IL (2), correlating with the corresponding RDF data (g_{C-A}), attributing the strong electrostatic interaction between cations and anions, thus affecting the mobility of the fluoride ions.

2.3.2. Stability of DMAP ILs (2) and (3). Thermal stability of ionic liquids directs their applications in a number of industrial processes, therefore the evaluation of thermal stabilities of DMAP based ionic liquids was carried out in terms of binding energies. The energy data was obtained by the application of MP2 method on the HF optimized structures of DMAP ILs (2) and (3). A very close value of binding energies was obtained as listed in Table 2. Binding energy data obtained from the *ab*

Table 2 Binding energies of DMAP based ionic liquids obtained from MP2 calculations

DMAP-ILs	2	3
Energy (kcal mol^{-1})	131.3	131.2

initio calculations was in excellent agreement with the thermogravimetric analysis for DMAP ILs (2) and (3) which yielded respective optimal decomposition temperatures of 265 and 260 °C thus showing identical stability of these compounds. The correlation between structural properties and thermodynamics properties in terms of radial distribution functions and binding energies of DMAP based ionic liquids was observed, since both the structural and thermodynamics properties of the two ionic liquids were very close yet differences in the self-diffusion coefficients for cations and anions indicated the influence of side chain dynamics on the transport properties. The influence of the side chain on the diffusion coefficients were correlated to gyration radius which clearly shows the difference in the side chain dynamics affecting the diffusion of cations and anions. Self-diffusion coefficients were reported to be linearly varied with the alkyl chain lengths[38] but anomalies could be expected.

3. Conclusion

In conclusion, two new ionic liquids (2, 3), based on *N,N*-dimethylpyridin-4-amine (DMAP) as head group have been synthesized and successfully employed as catalysts for the preparation of indole/indolenine *via* Fischer indole synthesis, and 1*H*-phenyl tetrazoles *via* click chemistry. The wide scope of use of newly synthesized DMAP-ILs as efficient catalyst was established by synthesizing series of different indoles (7–14), and tetrazoles (17–22) in good yields (up to 89%). The reduced toxicity of DMAP, as compared to pyridine offers advantages in preparation of DMAP-IL and handling in organic reactions. Low catalyst loading (0.2 equiv.) further adds to advantages in terms of its facile removal from the reaction mixture during the purification process. In addition, thermal stability of DMAP based catalysts 2 and 3 has been demonstrated *via* TGA, DTG and DSC studies. The first successful application of new DMAP-ILs in Fisher indole and 1*H*-tetrazole synthesis signifies their importance in organic syntheses. MD simulation provided detailed insights into the anomalous behavior of the transport properties of similar DMAP based ionic liquids. Large negative values of binding energies demonstrated the stability of these compounds which were corroborated with decomposition temperature obtained from thermogravimetric analysis.

4. Material and methods

N,N-Dimethylpyridin-4-amine (DMAP) (≥99.0%), pentyl bromide, heptyl bromide, toluene (≥99.5%), potassium fluoride (≥99.0%) were purchased from Sigma Aldrich and used without any purification unless otherwise stated. Thin layer chromatography (TLC) was carried out using silica gel 60 aluminium-backed plates 0.063–0.200 mm. Analytical grade solvents such as ethyl acetate (EtOAc), diethyl ether, hexane and methanol *etc.* were used. Short wavelength UV radiation at 254 nm was used for visualization of TLC plates. Staining mixture such as basic potassium permanganate or vanillin were also used for visualization of TLC plates. Infrared (IR) spectra were recorded on Bruker Vector-22 spectrometer. The ^1H NMR spectra were recorded on Bruker spectrometers at 300 MHz, 400

MHz, 500 MHz, and 600 MHz, while ^{13}C NMR spectra were recorded at 75 MHz, 100 MHz, 125 MHz, 150 MHz in deuterated solvents. The chemical shifts were recorded on the δ-scale (ppm) using residual solvents as an internal standard (DMSO; ^{1}H 2.50, ^{13}C 39.43 and CHCl$_3$; ^{1}H 7.26, ^{13}C 77.16). Coupling constants were calculated in hertz (Hz) and multiplicities were labelled s (singlet), d (doublet), t (triplet), q (quartet), quint (quintet) and the prefixes br (broad) or app (apparent) were used. Mass spectra (EI$^+$ and FAB) were recorded on Finnigan MAT-321A, Germany. Melting points of solids were determined using a Stuart™ melting point SMP3 apparatus.

4.1. General synthetic procedure for DMAP-based ionic fluoride salts (2, 3)

An over dried round bottomed flask was cooled to room temperature and charged with N,N-dimethylpyridin-4-amine (500 mg, 4.09 mmol, 1 equiv.), toluene (5 mL), and corresponding alkyl bromide (1 equiv.) at room temperature. The reaction mixture was heated at reflux (118–120 °C) for 2 to 12 h until no starting material was observed on TLC analysis. On cooling the resulting ionic salts, as oily solid which after some time became thick oil, was separated and washed further with cooled toluene and dried *in vacuo*. The obtained crude ionic liquids were treated with aqueous solution of silver fluoride (4–5 mL, 1 equiv.). Afterward, the precipitates of silver bromide were removed by filtration and then water was evaporated with freeze drying process. The resulting residue was dissolved in chloroform, filtered and evaporated on rotary evaporator. The obtained materials were occasionally washed with cooled toluene or hexane to get the final desired products DMAP-ILs (2 and 3). The obtained DMAP-ILs 2 and 3 were fully characterized with ^{1}H, ^{13}C-NMR, IR, UV spectroscopy and mass spectrometry.

4.2. Spectral data of DMAP-based ionic fluoride salts

4.2.1. 4-(Dimethylamino)-1-pentylpyridin-1-ium fluoride (2). Light yellow oil, (165 mg, 78%). ^{1}H NMR (400 MHz, DMSO-d_6): δ_H 8.28 (2H, d, J = 7.6 Hz, ArH), 7.02 (2H, d, J = 7.6 Hz, ArH), 4.14 (2H, t, J = 7.2 Hz, CH$_2$), 3.17 (6H, s, C(CH$_3$)$_2$), 1.75 (2H, quint, J = 7.4 Hz, CH$_2$), 1.28 (2H, app quint, J = 7.4 Hz, CH$_2$), 1.18 (2H, app quint, J = 7.4 Hz, CH$_2$), 0.85 (3H, t, 7.2 Hz, CH$_3$); ^{13}C NMR (100 MHz, DMSO-d_6): δ_C 155.8 (C), 141.9 (CH ×2), 107.6 (CH ×2), 56.6 (CH$_2$), 39.7 (CH$_3$ ×2), 29.9 (CH$_2$), 27.5 (CH$_2$), 21.5 (CH$_2$), 13.8 (CH$_3$). ^{19}F NMR (400 MHz, CD$_3$CN): δ_F −127.4. MS-EI m/z, 193.2 (M$^+$ − F$^-$). EI-HRMS (M$^+$ − F$^-$) C$_{12}$H$_{21}$N$_2$ found 193.1722, calculated 193.1705.

4.2.2. 4-(Dimethylamino)-1-heptylpyridin-1-ium fluoride (3). Yellow oil, (180 mg, 75%). IR (ν_{max}, cm^{-1}): (liquid, CHCl$_3$) 3442, 2929, 1650, 1569, 1403, 1175, 833. ^{1}H NMR (400 MHz, DMSO-d_6): δ_H 8.31 (2H, d, J = 8.0 Hz, ArH), 7.02 (2H, d, J = 7.6 Hz, ArH), 4.15 (2H, t, J = 7.0 Hz, CH$_2$), 3.17 (6H, s, C(CH$_3$)$_2$), 1.75 (2H, quint, J = 7.4 Hz, CH$_2$), 1.27–1.19 (8H, m, (CH$_2$)$_4$), 0.85 (3H, t, J = 6.6 Hz, CH$_3$); ^{13}C NMR (100 MHz, DMSO-d_6): δ_C 155.8 (C), 142.1 (CH ×2), 107.7 (CH ×2), 56.6 (CH$_2$), 39.7 (CH$_3$ ×2), 31.1 (CH$_2$), 30.3 (CH$_2$), 28.1 (CH$_2$), 25.3 (CH$_2$), 21.9 (CH$_2$), 13.8 (CH$_3$). ^{19}F NMR (400 MHz, CD$_3$CN): δ_F −127.5. MS-ESI m/z (%),

221.1 (M$^+$ − F$^-$), 220, 219; EI-HRMS (M$^+$ − F$^-$) C$_{14}$H$_{25}$N$_2$ found 221.1999, calculated 221.2018.

4.3. Procedure for substituted tetrahydro-1*H*-carbazole (indoles)/methyl tetrahydro-1*H*-carbazole (indolenines) synthesis

In a general procedure, an oven dried round bottomed flask was charged with corresponding phenyl hydrazine hydrochloride (1 mmol, 1 equiv.) and ethanol (3 mL). To the resulting solution corresponding cyclohexanone/methyl cyclohexanone (1 mmol, 1 equiv.) and 4-(dimethylamino)-1-pentylpyridin-1-ium fluoride (2) (0.2 mmol, 0.2 equiv.) was added at room temperature and mixture was heated at reflux (78–80 °C) under nitrogen atmosphere. The consumption of starting material was monitored by thin layered chromatography by using eluents ethyl acetate/hexane (3 : 7). The crude reaction mixture was directly purified by silica gel column chromatography by using eluents in gradient eluents EtOAc/hexane (1 : 9 to 1 : 1) to get the corresponding pure products (6a–h) in different yields.

4.3.1. 2,3,4,9-Tetrahydro-1*H*-carbazole (6a). Yield 89% ^{1}H NMR (400 MHz, DMSO-d_6): δ_H 10.58 (1H, s, NH), 7.30 (1H, d, J = 7.6 Hz, ArH), 7.20 (1H, d, J = 8 Hz, ArH), 6.96 (1H, t, J = 7.2 Hz, ArH), 6.89 (1H, t, J = 7.6 Hz, ArH), 2.68 (2H, t, J = 5.6 Hz, CH$_2$), 2.60 (2H, t, J = 5.4 Hz, CH$_2$), 1.82–1.79 (4H, m, (CH$_2$)$_2$); MS-EI m/z 171.1 (M$^+$). The data is identical to those previously reported.[39]

4.3.2. 6-Methoxy-2,3,4,9-tetrahydro-1*H*-carbazole (6b).[39] Yield 78% ^{1}H NMR (400 MHz, DMSO): δ_H 10.39 (1H, s, NH), 7.10 (1H, d, J = 8.8 Hz, ArH), 6.81 (1H, d, J = 2.0 Hz, ArH), 6.59 (1H, dd, J = 8.4, 2.4 Hz, ArH), 3.71 (1H, s, OCH$_3$), 2.63 (2H, t, J = 5.6 Hz, CH$_2$), 2.60 (2H, t, J = 5.6 Hz, CH$_2$), 1.79–1.77 (4H, m, (CH$_2$)$_2$); MS-EI m/z 201 (M$^+$).

4.3.3. 6-Fluoro-2,3,4,9-tetrahydro-1*H*-carbazole (6c).[40,41] Yield 74% ^{1}H NMR (300 MHz, DMSO-d_6): δ_H 10.69 (1H, s, NH), 7.19 (1H, dd, J = 8.4, 3.8 Hz, ArH), 7.04 (1H, dd, J = 10.0, 2.4 Hz, ArH), 6.76 (1H, td, J = 9.6, 2.7 Hz, ArH), 2.67 (2H, t, J = 5.4 Hz, CH$_2$), 2.56 (2H, t, J = 5.4 Hz, CH$_2$), 1.82–1.75 (4H, m, CH$_2$–CH$_2$). MS-EI m/z 189.1 (M$^+$).

4.3.4. 6-Methoxy-1-methyl-2,3,4,9-tetrahydro-1*H*-carbazole (6d). Yield 56% ^{1}H NMR (400 MHz, DMSO-d_6): δ_H 11.55 (1H, s, NH), 7.33 (1H, d, J = 8.4 Hz, ArH), 6.99 (1H, d, J = 2.4 Hz, ArH), 6.86 (1H, dd, J = 8.4, 2.4 Hz, ArH), 3.76 (3H, s, OCH$_3$), 2.86–2.82 (1H, m, CH), 2.08 (1H, m, CHH), 1.81–1.78 (1H, m, CHH), 1.55 (1H, m, CH$_2$–CHH), 1.22 (3H, d, J = 6.4 Hz, CH$_3$), 1.19–1.03 (3H, m, CH$_2$–CHH). MS-EI m/z 215.1 (M$^+$), EI-HRMS (M$^+$) C$_{14}$H$_{17}$N$_1$O found 215.1327, calculated 215.1310.

4.3.5. 8-Chloro-4*a*-methyl-2,3,4,4*a*-tetrahydro-1*H*-carbazole (6e). Yield 76% ^{1}H NMR (400 MHz, DMSO-d_6): δ_H 7.38 (1H, d, J = 7.2 Hz, ArH), 7.34 (1H, d, J = 8 Hz, ArH), 7.19 (1H, t, J = 7.6 Hz, ArH), 2.71 (1H, app d, J = 12.8 Hz, CHH), 2.66–2.58 (1H, m, CHH), 2.27 (1H, app d, J = 13.2 Hz, CHH), 2.13 (1H, app d, J = 13.2 Hz, CHH), 1.80–1.72 (1H, m, CHH–CH$_2$), 1.60 (1H, app d, J = 13.6 Hz, CHH–CH$_2$), 1.34–1.26 (1H, m, CH$_2$–CHH), 1.27 (3H, s, CH$_3$), 1.01 (1H, td, J = 13.2, 4 Hz, CH$_2$–CHH). MS-EI m/z 219.1 (M$^+$), 221.1, EI-HRMS (M$^+$) C$_{13}$H$_{14}$N$_1$Cl found 219.0811, calculated 219.0815.

4.3.6. 6-Cyano-2,3,4,9-tetrahydro-1H-carbazole (6f). Yield 60% ^{1}H NMR (300 MHz, DMSO-d_6): δ_H 11.27 (1H, s, NH), 7.83 (1H, s, ArH), 7.38 (1H, d, J = 8.4 Hz, ArH), 7.31 (1H, dd, J = 8.4, 1.5 Hz, ArH), 2.69 (2H, app t, J = 6.4 Hz, CH$_2$), 2.64 (2H, t, J = 5.7 Hz, CH$_2$), 1.81–1.74 (4H, m, CH$_2$–CH$_2$). MS-EI m/z 196.1 (M$^+$).

4.3.7. 7-Bromo-4a-methyl-2,3,4,4a-tetrahydro-1H-carbazole (6g). Yield 55% ^{1}H NMR (400 MHz, DMSO-d_6): δ_H 7.65 (1H, s J = 7.6 Hz, ArH), 7.39–7.34 (2H, m, ArH), 7.64 (1H, d, J = 8 Hz, ArH), 2.68–2.57 (2H, m, CH$_2$), 2.28 (1H, app dd, J = 12.8, 2.4 Hz, CHH), 2.12 (1H, app d, J = 12.8 Hz, CHH), 1.79–1.71 (1H, m, CHH–CH$_2$), 1.60 (1H, app d, J = 14 Hz, CHH–CH$_2$), 1.31–1.21 (CHH–CH$_2$), 1.24 (3H, s, CH$_3$), 0.97 (1H, td, J = 13.6, 4 Hz, CH$_2$–CHH). MS-EI m/z 263.2 (M$^+$), 265.2, EI-HRMS (M$^+$) C$_{13}$H$_{14}$N$_1$Br found 263.0300, calculated 263.0310.

4.3.8. 6-Methoxy-2,2-dimethyl-2,3-dihydro-1H-carbazol-4-(9H)-one (6h).[42] Yield 17% ^{1}H NMR (400 MHz, DMSO-d_6): δ_H 11.66 (1H, s, NH), 7.43 (1H, d, J = 2.4 Hz, ArH), 7.25 (1H, d, J = 8.8 Hz, ArH), 6.76 (1H, t, J = 8.8 Hz, ArH), 3.75 (3H, s, OCH$_3$), 2.80 (2H, s, CH$_2$), 2.30 (2H, s, CH$_2$), 1.07 (6H, s, (CH$_3$)$_2$).

4.4. A general procedure for phenyl 1H-tetrazole synthesis

To an oven dried micro reaction vessel corresponding benzonitrile (1 mmol, 1 equiv.), trimethylsilyl azide (3 mmol, 3 equiv.) and DMAP-IL **5** (0.3 equiv.) were added at room temperature and then capped with septum for reaction. The vessel with reaction mixture was heated at 110–115 °C for 24 h until the complete consumption of starting material, judged thin layer chromatography. On cooling the reaction mixture was diluted with EtOAc (20 mL) and shaked with 1–2 M HCl (20 mL) in separating funnel. Organic layer was separated and aqueous layer was further extracted with EtOAc (15 mL). The combined organic layers were dried with MgSO$_4$, filter and evaporated *in vacuo* to get the crude material. For purification silica gel column chromatography with eluents EtOAc/hexane (1 : 1) to get the pure 1H-tetrazoles (**17–22**) as off-white to white solids in 48–78% yield.

4.4.1. 5-Phenyl-1H-tetrazole (17). 48% ^{1}H NMR (400 MHz, DMSO-d_6): δ_H 8.04–8.02 (2H, m, ArH), 7.60–7.58 (3H, m, ArH); MS-EI m/z 146 (M$^+$). The data is identical to those previously reported.[15]

4.4.2. 5-(4′-Methylphenyl)-1H-tetrazole (18).[43] 78% ^{1}H NMR (400 MHz, DMSO-d_6): δ_H 7.91 (2H, d, J = 8.4 Hz, ArH), 7.39 (2H, d, J = 8.0 Hz, ArH), 2.38 (3H, s, CH$_3$); MS-EI m/z 160 (M$^+$).

4.4.3. 5-(4′-Chlorophenyl)-1H-tetrazole (19).[43,44] 59% ^{1}H NMR (400 MHz, DMSO-d_6): δ_H 8.06 (2H, d, J = 8.4 Hz, ArH), 7.68 (2H, d, J = 8.4 Hz, ArH); MS-EI m/z 180 (M$^+$).

4.4.4. 5-(4′-Bromophenyl)-1H-tetrazole (20).[43] 68% ^{1}H NMR (400 MHz, DMSO-d_6): δ_H 7.96 (2H, d, J = 8.4 Hz, ArH), 7.79 (2H, d, J = 8.4 Hz, ArH); MS-EI m/z 223 (M$^+$), 225.

4.4.5. 5-(4′-Methoxyphenyl)-1H-tetrazole (21).[45] 70% ^{1}H NMR (400 MHz, DMSO-d_6): δ_H 7.97 (2H, d, J = 8.8 Hz, ArH), 7.14 (2H, d, J = 8.8 Hz, ArH), 3.83 (3H, s, OCH$_3$); MS-EI m/z 176 (M$^+$).

4.4.6. 5-(4′-Fluorophenyl)-1H-tetrazole (22).[46] 58% ^{1}H NMR (400 MHz, DMSO-d_6): δ_H 8.07 (2H, dd, J = 8.8, 5.6 Hz, ArH), 7.45 (2H, t, J = 8.8 Hz, ArH); MS-EI m/z 164 (M$^+$).

4.5. Theoretical methods

A similar protocol was followed for the theoretical investigation of DMAP based ionic liquids that was successfully applied to quinolone based ionic fluoride salts (QuFs).[36]

4.5.1. Binding energy calculations. Prior to binding energy calculations, both DMAP (**2**) and (**3**) derivatives were optimized at the Hartree–Fock level of theory using 6-311G(d,p) basis sets for all atoms without the application of symmetry constraints. The binding energies of both derivatives were calculated at MP2 level of theory and 6-311G(d,p) basis sets were utilized for all atoms in order to evaluate thermal stabilities of these compounds. All *ab initio* calculations were performed using Gaussian 09 software.[47]

4.5.2. Molecular dynamics simulations. The initial configuration of the simulation boxes of DMAP (**2**) and (**3**) ionic liquids were prepared using the optimized structures of these derivatives as shown Fig. 9.

Both DMAP derivatives were modeled with Generalized Amber Force Field (GAFF)[48] and restrained electrostatic potential (RESP) charges[49,50] were obtained. Simulation boxes consisting of 200 ion pairs of DMAP derivatives were constructed in defined regions of space using Packmol program.[51]

Prior to performing MD simulations, both systems were subjected to 10 000 steps of energy minimizations which were then followed by NVT equilibration for 15 ns. Afterwards, both systems were subjected to production MD for 40 ns including NPT equilibration and sampling of simulation trajectories. All bonds including hydrogen bonds were kept, thus enabling to use time step of 1.0 fs throughout the simulation. Long range electrostatic interactions were treated by applying particle mesh Ewald algorithm and for non-bonded interactions, a cutoff value of 8.0 Å was used. The temperature was controlled at ∼298 K using Langevin thermostat with collision frequency of 5.0 ps^{-1}, and pressure coupling algorithm with a relaxation time pf 1.0 ps was employed to maintain the pressure. Both MD simulation were performed using SANDER module of AMBERTOOLS17 whereas analysis of simulation trajectories were
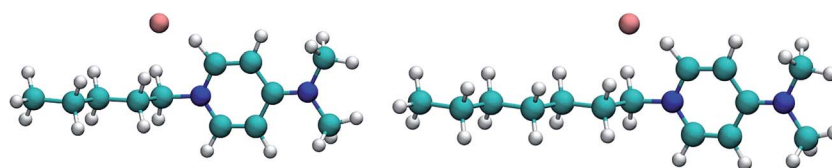

Fig. 9 HF optimized structures of DMAP (**2**) and (**3**) ionic liquids.

carried out by the CPPTRAJ module of AMBERTOOLS17.[52] For the visualization of simulation trajectories, VMD[53] were used.

Conflict of interest

The authors have declared no conflict of interest.

Acknowledgements

References

1 T. Welton, *Chem. Rev.*, 1999, **99**, 2071–2084.

2 P. Wasserscheid and T. Welton, *Ionic liquids in synthesis*, John Wiley & Sons, 2008.

3 J. P. Hallett and T. Welton, *Chem. Rev.*, 2011, **111**, 3508–3576.

4 N. V. Plechkova and K. R. Seddon, *Chem. Soc. Rev.*, 2008, **37**, 123–150.

5 R. D. Rogers, K. R. Seddon and S. Volkov, *Green industrial applications of ionic liquids*, Springer Science & Business Media, 2012.

6 V. G. Rao, C. Banerjee, S. Ghosh, S. Mandal, J. Kuchlyan and N. Sarkar, *J. Phys. Chem. B*, 2013, **117**, 7472–7480.

7 H. Niedermeyer, J. P. Hallett, I. J. Villar-Garcia, P. A. Hunt and T. Welton, *Chem. Soc. Rev.*, 2012, **41**, 7780–7802.

8 M. Freemantle, *An introduction to ionic liquids*, Royal Society of Chemistry, 2009.

9 R. L. Vekariya, *J. Mol. Liq.*, 2016, **227**, 44–60.

10 X. Chen and A. Ying, *DBU derived ionic liquids and their application in organic synthetic reactions*, INTECH Open Access Publisher, 2011.

11 G. Sabitha, N. M. Reddy, M. N. Prasad and J. S. Yadav, *Helv. Chim. Acta*, 2009, **92**, 967–976.

12 G. Kumaraswamy and A. Pitchaiah, *Helv. Chim. Acta*, 2011, **94**, 1543–1550.

13 J. H. Clark, *Chem. Rev.*, 1980, **80**, 429–452.

14 A. Hameed, R. D. Alharthy, J. Iqbal and P. Langer, *Tetrahedron*, 2016, **72**, 2763–2812.

15 D. Amantini, R. Beleggia, F. Fringuelli, F. Pizzo and L. Vaccaro, *J. Org. Chem.*, 2004, **69**, 2896–2898.

16 R. Sundberg, *The chemistry of indoles*, Academic Press, New York and London, 2012.

17 D.-Q. Xu, J. Wu, S.-P. Luo, J.-X. Zhang, J.-Y. Wu, X.-H. Du and Z.-Y. Xu, *Green Chem.*, 2009, **11**, 1239–1246.

18 G. L. Rebeiro and B. M. Khadilkar, *Synthesis*, 2001, **2001**, 0370–0372.

19 S. Gore, S. Baskaran and B. König, *Org. Lett.*, 2012, **14**, 4568–4571.

20 M. Malik, M. Wani, S. Al-Thabaiti and R. Shiekh, *J. Inclusion Phenom. Macrocyclic Chem.*, 2014, **78**, 15–37.

21 L. V. Myznikov, A. Hrabalek and G. I. Koldobskii, *Chem. Heterocycl. Compd.*, 2007, **43**, 1–9.

22 S. J. Wittenberger, *Org. Prep. Proced. Int.*, 1994, **26**, 499–531.

23 R. N. Butler, in *Comprehensive heterocyclic chemistry II*, ed. A. R. Katritzky, C. W. Rees and E. F. V. Scriven, Pergamon, Oxford, 1996, pp. 621–678.

24 P. N. Gaponik, S. V. Voitekhovich and O. A. Ivashkevich, *Russ. Chem. Rev.*, 2006, **75**, 507.

25 R. J. Herr, *Bioorg. Med. Chem.*, 2002, **10**, 3379–3393.

26 A. Sarvary and A. Maleki, *Molec. Divers.*, 2015, **19**, 189–212.

27 A. Maleki and A. Sarvary, *RSC Adv.*, 2015, **5**, 60938–60955.

28 Z. P. Demko and K. B. Sharpless, *Angew. Chem., Int. Ed.*, 2002, **41**, 2110–2113.

29 Z. P. Demko and K. B. Sharpless, *J. Org. Chem.*, 2001, **66**, 7945–7950.

30 S. Vorona, T. Artamonova, Y. Zevatskii and L. Myznikov, *Synthesis*, 2014, **46**, 781–786.

31 S. Hajra, D. Sinha and M. Bhowmick, *J. Org. Chem.*, 2007, **72**, 1852–1855.

32 E. J. Maginn, *Acc. Chem. Res.*, 2007, **40**, 1200–1207.

33 N. Stolwijk and S. Obeidi, *Electrochim. Acta*, 2009, **54**, 1645–1653.

34 M. Kowsari, S. Alavi, B. Najafi, K. Gholizadeh, E. Dehghanpisheh and F. Ranjbar, *Phys. Chem. Chem. Phys.*, 2011, **13**, 8826–8837.

35 A. T. Nasrabadi and L. D. Gelb, *J. Phys. Chem. B*, 2017, **121**, 1908–1921.

36 N. Iqbal, J. Hashim, S. A. Ali, M. al-Rashida, R. D. Alharthy, S. Ahmad, K. M. Khan, F. Z. Basha, S. T. Moin and A. Hameed, *RSC Adv.*, 2015, **5**, 95061–95072.

37 P. G. M. Wuts and T. W. Greene, *Greene's Protective Groups in Organic Synthesis*, Wiley, 2006.

38 H. Tokuda, K. Hayamizu, K. Ishii, M. A. B. H. Susan and M. Watanabe, *J. Phys. Chem. B*, 2005, **109**, 6103–6110.

39 S. Gore, S. Baskaran and B. König, *Org. Lett.*, 2012, **14**, 4568–4571.

40 P. P. Varma, B. S. Sherigara, K. M. Mahadevan and V. Hulikal, *Synth. Commun.*, 2008, **39**, 158–165.

41 S. Chandrasekhar and S. Mukherjee, *Synth. Commun.*, 2015, **45**, 1018–1022.

42 D.-Q. Xu, J. Wu, S.-P. Luo, J.-X. Zhang, J.-Y. Wu, X.-H. Du and Z.-Y. Xu, *Green Chem.*, 2009, **11**, 1239–1246.

43 H. Naeimi and S. Mohamadabadi, *Dalton Trans.*, 2014, **43**, 12967–12973.

44 V. Rama, K. Kanagaraj and K. Pitchumani, *J. Org. Chem.*, 2011, **76**, 9090–9095.

45 O. Marvi, A. Alizadeh and S. Zarrabi, *Bull. Korean Chem. Soc.*, 2011, **32**, 4001.

46 Z. Du, C. Si, Y. Li, Y. Wang and J. Lu, *Int. J. Mol. Sci.*, 2012, **13**, 4696–4703.

47 M. Frisch, G. Trucks, H. Schlegel, G. Scuseria, M. Robb, J. Cheeseman, G. Scalmani, V. Barone, B. Mennucci and G. Petersson, *Gaussian 09*, Gaussian, Inc., Wallingford CT, 2009.

48 J. Wang, R. M. Wolf, J. W. Caldwell, P. A. Kollman and D. A. Case, *J. Comput. Chem.*, 2004, **25**, 1157–1174.

49 C. I. Bayly, P. Cieplak, W. Cornell and P. A. Kollman, *J. Phys. Chem.*, 1993, **97**, 10269–10280.

50 P. Cieplak, W. D. Cornell, C. Bayly and P. A. Kollman, *J. Comput. Chem.*, 1995, **16**, 1357–1377.

51 L. Martínez, R. Andrade, E. G. Birgin and J. M. Martínez, *J. Comput. Chem.*, 2009, **30**, 2157–2164.

52 D. A. Case, T. E. Cheatham, T. Darden, H. Gohlke, R. Luo, K. M. Merz, A. Onufriev, C. Simmerling, B. Wang and R. J. Woods, *AMBER 17, Report 1096-987X*, University of California, San Francisco, 2017.

53 W. Humphrey, A. Dalke and K. Schulten, *J. Mol. Graphics*, 1996, **14**, 33–38.